Game Theory Controller for Hybrid Electric Vehicles

Clément Dextreit and Ilya V. Kolmanovsky, *Fellow, IEEE*

***Abstract*— This paper describes the development and experimental implementation of an energy management controller for hybrid electric vehicles (HEVs) based on the application of game theory (GT). This controller is constructed as a feedback Stackelberg equilibrium in the noncooperative game between the driver and the powertrain with the cost penalizing fuel consumption, NO_x emissions, battery state of charge deviation, and vehicle operating conditions deviation. This control policy is drive-cycle and time independent. A description of the controller implementation with ancillary strategy elements is given. Experimental results from tests in a parallel HEV prototype vehicle are presented and compared with the existing baseline controller in terms of fuel consumption and NO_x emissions. The HEV powertrain configuration is advanced and includes a high-speed diesel engine, two electric motors, and automated converterless transmission. Over the New European Driving Cycle (NEDC), the GT controller, with minimal calibration effort, demonstrates better performance than the existing baseline controller that is calibrated from the deterministic dynamic programing solution over NEDC. We also demonstrate that the GT controller substantially outperforms the baseline controller over other real-world-focused driving cycles while providing good drivability.**

***Index Terms*— Diesel engines, emissions, energy management, game theory, hybrid electric vehicles (HEVs), optimal control.**

I. Introduction

HYBRID electric vehicles (HEVs) [7], [13] are gaining market popularity concomitantly with rising fuel prices. Unlike conventional vehicles, in typical HEVs, there are multiple degrees of freedom for delivering wheel torque [19]. In a parallel HEV, the wheel power can be delivered by various combinations of the mechanical engine power and the electric motor or battery power. The term "HEV energy and emissions management" generally refers to policies for allocating the wheel torque to available power sources. Policies that maximize average fuel economy, control average emissions within legislative constraints, and sustain on average battery state of charge (SoC) are of particular interest for HEVs. Reference [15] surveys several existing approaches to HEV energy management; see also [5], [6], [18], [20], [22], [30], [31], [34], [35] and references therein. The focus of this paper is on energy management for HEVs that are similar to the Freelander2 vehicle in Fig. 1. The HEV powertrain is based on a diesel engine as a primary energy source and two electric motors. The first electric motor is integrated with the engine crankshaft and the second motor is integrated with the rear wheels. The energy management policies for this advanced HEV powertrain must lower fuel consumption and satisfy constraints on oxides of nitrogen (NO_x) emissions without compromising vehicle drivability. This engine has a diesel particulate filter that is periodically regenerated but no exhaust after treatment system for NO_x. Therefore, NO_x emissions reduction at the exhaust level is critical to enable this vehicle to meet emissions regulations.

Fig. 1. Jaguar Land Rover Freelander2 HEV.

In this paper, we report on the development, implementation, and testing in a parallel HEV prototype of an energy management strategy based on the application of game theory (GT). In this approach, the vehicle operating conditions (wheel speed and wheel torque) and the powertrain are viewed as two players in a finite-horizon noncooperative game. A cost functional of this game weights fuel consumption, NO_x emissions, the deviation of SoC of the battery from the set-point, and the deviation of vehicle operating conditions from the nominal operating conditions. The policy for deciding the mode to control battery, motors, and engine power output is constructed as a function of wheel torque, wheel speed, and SoC of the battery.

The contributions of this paper are as follows. First, we describe the detailed application and implementation of the novel GT approach for HEV powertrain energy and emissions management. Second, we treat an advanced parallel HEV powertrain with a diesel engine and two electric motors. Unlike most papers on the subject, we treat not only fuel consumption

Manuscript received May 15, 2012; accepted February 23, 2013. Manuscript received in final form March 20, 2013. Date of publication April 30, 2013; date of current version February 14, 2014. Recommended by Associate Editor U. Christen.

C. Dextreit is with Jaguar Land Rover, Gaydon CV35 ORR, U.K. (e-mail: cdextrei@jaguarlandrover.com).

I. V. Kolmanovsky is with the Department of Aerospace Engineering, University of Michigan, Ann Arbor, MI 48109 USA (e-mail: ilya@umich.edu).

Color versions of one or more of the figures in this paper are available online at http://ieeexplore.ieee.org.

Digital Object Identifier 10.1109/TCST.2013.2254597

but also NO_x emissions in the optimization. Third, we present experimental results from the prototype vehicle which demonstrate that the GT controller, with minimal calibration effort, exceeds the performance of the baseline controller calibrated from the deterministic dynamic programing (DDP) solution over the New European Drive-Cycle (NEDC). We also show that the GT controller outperforms the baseline controller over other real-world-focused driving cycles.

Preliminary results were reported in our conference papers [10]–[12]. In particular, in [10] and [11], detailed vehicle model simulations were used to establish that the GT-based solution can outperform the stochastic dynamic programing (SDP)-based solution and two conventional energy management strategies in terms of fuel economy. This paper briefly summarizes the results of [10] and [11] and reports implementation details and results not discussed in our shorter and preliminary conference paper [12].

This paper is organized as follows. In Section II, we review several existing approaches to HEV energy management that are based on related dynamic programing ideas. In Section III, we introduce the GT approach and contrast it with the dynamic programing approaches of Section II. In Section IV, we describe the architecture of the HEV prototype. In Section V, we briefly summarize the results of the previous fuel economy assessment in [11] that motivated us to retain the GT controller and a particular baseline controller for further development and evaluation. In Section VI, we provide a description of the model-based desktop optimization setup used to generate the DDP and GT solutions. The baseline controller [battery optimal power output map (BOPOM)] and its calibration are discussed in Section VII. The implementation details and testing results for the GT controller are described in Section VIII. Finally, concluding remarks are made in Section IX.

II. Dynamic Optimization of HEV Energy Management

Several approaches to dynamic optimization of powertrain operation were proposed in prior literature. These approaches are typically applied to a discrete-time dynamic system model of the form

$$x(t+1) = f(x(t), u(t), w(t)) \tag{1}$$

where $x(t)$ is the state vector, $u(t)$ is the control vector, and $w(t)$ is a vector of operating conditions.

Dynamic optimization approaches proposed in the literature differ primarily in their assumptions on $w(t)$ which in these applications correspond to the vector of wheel speed and wheel torque request. The control objective is to determine a policy that minimizes the cost functional of the form

$$J = K(x(T), w(T)) + \sum_{t=0}^{T-1} L(x(t), u(t), w(t)). \tag{2}$$

Cost (2) typically penalizes fuel consumption and deviations of the battery SoC. In the majority of the existing literature, and unlike this paper, the treatment does not include HEV non-CO_2 emissions. As our powertrain is based on a diesel engine without NO_x after treatment, the reduction of NO_x emissions is very important. Hence, NO_x emissions are included in (2) in this paper. The functions K and L in (2) are referred to as the terminal cost function and the incremental cost function, respectively.

In DDP [3], $w(t)$, $t = 0, \ldots, T$, is prescribed by a specific driving cycle such as NEDC. The resulting control policy, $u(t) = U_{dp}(x(t), t)$, is state and time dependent. The DDP-based control policies are previously used for: 1) assessing the best achievable performance of a given powertrain over a given drive-cycle and 2) calibrating parameters of a conventional, rule-based (RB) control policy to replicate the optimal state and control trajectories generated by the DDP policy. First applications of DDP to powertrain control appear to be [1], [9], [21]. Brahma *et al.* [5] describes the first application of DDP to HEV energy management. References [32] and [33] exploit approximate dynamic programing actor-critic techniques [4] to train HEV control policies. Kang *et al.* [21] proposes that the approach of applying DDP to constant drive-cycle profiles (i.e., with $w(t) = \text{const}$) and subsequently interpolating the resulting optimal policies can lead to reasonable suboptimal and drive-cycle independent control policies. By drive-cycle independence, here and throughout, we refer to control policies that are not developed, assuming precise knowledge of future vehicle speed trajectory and road to come [25], [26].

As the control policy resulting from the DDP approach is drive-cycle dependent, the SDP approach is proposed [3] to alleviate the drive-cycle dependency of the control policy. In SDP, $w(t)$ is modeled as a Markov chain stochastic process and a control policy is determined in the time-independent form, $u = U_{\text{sdp}}(x, w)$, as a solution to an infinite-horizon discounted version of (2). The transition probabilities of the Markov chain for $w(t)$ are identified from the operating condition trajectories over one or more drive-cycles. The principal disadvantage of the SDP policies is dependence on the assumption of a Markov process model for $w(t)$ and higher complexity (versus DDP) of their offline generation. Specifically, the value (cost-to-go) that is constructed via value function iterations depends not only on $x(t)$, but also on $w(t)$.

The SDP approach to optimize the operating policy for powertrains with storage elements (of which HEV is a particular example) was proposed in [26]. [28] appears to be the first application of SDP to HEV operating policy optimization. [36] augments the Markov chain model with an absorbing state corresponding to the vehicle key-off state. Therefore, the discount factor is not needed, and flexibility is gained to select the form of the cost functional that promotes charge sustainability when the vehicle is likely to transition into a key-off state, and the problem of finding a value function can be recast as a large-scale linear programing problem. For other extensions and applications of SDP approach, see also [16], [17], [30] and references therein.

The equivalent consumption minimization strategy (ECMS) [15], [8] has also emerged as a popular method for HEV energy management. In the existing literature, ECMS is developed and justified based on Pontryagin's maximum principle applied to HEV dynamic optimization problems that

involve fuel consumption and battery charge sustainability requirements. This justification involves several simplifying assumptions. However, in our case, the powertrain is based on a diesel engine, and NO_x emissions reduction is critically important. The development of a (nonstandard) ECMS strategy, which includes not only the fuel economy but also NO_x emissions, for the purpose of comparing this approach with the GT approach, is beyond the scope of this paper and is left to future work. HEV control for NO_x reduction is also covered in [14].

III. GT Approach to HEV Energy Management

In the GT approach, $w(t) \in W$ is prescribed by the actions of the first player, which is responded to by the actions of the second player who prescribes the control, $u(t) \in U$. Here W, U denote, respectively, the sets from which the actions of the first player and the second player are selected. The players are engaged in a noncooperative game, and have competing objectives.

To relate this setup to our HEV application, the game takes place between the "driver," who selects powertrain operating variables $w(t)$ (e.g., a vector of wheel speed and wheel torque request), and the "powertrain" which selects powertrain control variables, $u(t)$. The state $x(t)$ is the SoC of the battery.

We employ the GT formulation to incorporate a representation of the driver actions to which the controller is to respond. In SDP or stochastic model predictive control (SMPC) approaches ([30], [34], and references therein), such a characterization is based on probabilistic scenarios. In our case, we optimize the response against the worst-case (in an appropriate sense) driving scenario and generate a robust response to different driving conditions. Our approach, based on noncooperative GT, is motivated by the fact that most of the drivers do not think or explicitly try to optimize their driving behavior for fuel economy and emissions while driving.

It is argued in [25] that the notion of feedback Stackelberg equilibria [15], [37] provides a suitable framework for formulating and solving the game problems relevant to powertrain control applications. This framework leads to a control policy, $u = U_{\mathrm{GT}}(x, w)$, which is a function of state and operating conditions only and is drive-cycle independent. The conceptual ideas and the computations involved in the construction of feedback Stackelberg equilibrium policies are now reviewed. See [2], [27], [37], and [38] for the background on GT and feedback Stackelberg equilibria.

Consider first a static two-player noncooperative game, where the first player (called the leader) wants to maximize a given objective function, $J(u, w)$, by selecting $w \in W$, whereas the second player (called the follower) wants to minimize it by selecting $u \in U$. The leader announces its move w first and then the follower reacts by selecting u. Assuming the follower reacts rationally, its strategy, $u = \hat{U}(w)$ must satisfy the following property:

$$J\left(\hat{U}(w), w\right) \leq J(u, w) \qquad \forall u \in U, w \in W.$$

The leader, assuming that the follower will react rationally, then picks a $w^* \in W$ satisfying

$$J\left(\hat{U}\left(w^*\right), w^*\right) \geq J\left(\hat{U}(w), w\right) \qquad \forall w \in W.$$

A pair, (w^*, u^*), $u^* \in \hat{U}(w^*)$, is called a Stackelberg equilibrium in the static game. Such a pair typically exists (e.g., under the assumptions of continuity of J and compactness of U and W), but may not be unique. Based on the above considerations such a pair satisfies

$$J\left(u^*, w^*\right) = \max_{w \in W} \min_{u \in U} J(u, w).$$

Consider next the case of a dynamic or a multistage game. Such a game is played for $(T-1)$ stages, where the number $(T-1)$ is referred to as the horizon of the game. In each stage of the game, each player is allowed one move, and the first player is the leader and the second player is the follower. Thus in the first stage of the game, given the initial state $x(0)$ but with no knowledge of the first move of the second player, $u(0)$, the first player selects $w(0)$. Then the second player, with the knowledge of $x(0)$ and $w(0)$ reacts by selecting its first move, $u(0)$. The state of (1) after the first stage is $x(1) = f(x(0), u(0), w(0))$. In the second stage of the game, the first player selects its second move, $w(1)$, with no knowledge of $u(1)$; the second player, with the knowledge of $w(1)$, reacts by selecting its second move, $u(1)$. The state of (1) after the second stage is $x(2) = f(x(1), u(1), w(1))$. The game is continued until all $(T-1)$ moves are completed.

The cost of the dynamic game is given by the functional $J(u(\cdot), w(\cdot))$ defined in (2). As in the static game, the objectives of the two players in the game are opposite with respect to this goal function. The first player wants to maximize it, whereas the second player wants to minimize it. Both players are assumed to behave rationally at each stage. A pair of sequences (u^*, w^*) constitutes a feedback Stackelberg equilibrium pair in the dynamic antagonistic game with the first player as the leader and the second player as the follower if $J(u^*(\cdot), w^*(\cdot)) = \max_{w(0)} \min_{u(0)} \max_{w(1)} \min_{u(1)}$

$$\cdots \max_{w(T-1)} \min_{u(T-1)} J(u(\cdot), w(\cdot)).$$

The value $J(u^*(\cdot), w^*(\cdot))$ is called the value of the game.

As in the optimal control problems, the optimal cost-to-go from a given stage t of the game can be described using a Bellman function defined by

$$V(x, t) = \max_{w(t)} \min_{u(t)} \max_{w(t+1)} \min_{u(t+1)} \cdots \max_{w(T-1)}$$
$$\min_{u(T-1)} \left\{ K(x(T), w(T)) + \sum_{k=t}^{T-1} L(x(k), u(k), w(k)) \right\}$$

where $x(k)$ evolves according to (1) with the initial condition $x(t) = x$. The domain of this function is $x \in X$ and $t = 0, \ldots, T$, and this function satisfies the equation similar to the Bellman equation, $V(x, t) = \max_{w \in W} \min_{u \in U} \{L(x, u, w, t) + V(f(x, u, w), t+1)\}$.

From the computational standpoint, the determination of optimal policies for the two players in such a game reduces to backward-in-stage cost-to-go-function updates, which are

similar to DDP updates as follows:

$$\hat{U}(x,w,t) = \{\hat{u} : \hat{u} \in \arg\min_{u\in U} \{L(x,u,w) + V(f(x,u,w),t+1)\}\}, \quad (3)$$

$$v(x,w,t) = \min_{u\in U}\{L(x,u,w) + V(f(x,u,w), t+1)\}, \quad (4)$$

$$\hat{W}(x,t) = \{\hat{w} : \hat{w} \in \arg\max_{w\in W}\{v(x,w,t)\}\}, \quad (5)$$

$$V(x,t) = \max_{w\in W}\min_{u\in U}\{L(x,u,w) + V(f(x,u,w), t+1)\}; t = T-1, T-2, \ldots, 0. \quad (6)$$

$$V(x,T) = \max_{w\in W}\min_{u\in U}\{K(x,u,w)\}. \quad (7)$$

The set of actions $\hat{U}(x,w,t)$ in (3) prescribes the optimal moves of the second player as a function of possible moves of the first player, w (not known to the second player in advance). Similarly, it is easy to see that $\hat{W}(x,t)$ in (5) prescribes the optimal moves of the first player as a function of the state of the system, x, and stage t, anticipating rational reaction of the second player to any move by the first player. Finally, (6) and (7) are the backward-in-stage updates of the "cost-to-go-function." Once the selections $\hat{U}(x,w,t)$, $\hat{W}(x,t)$ have been made, a pair $(u^*(\cdot), w^*(\cdot))$ satisfying $w^*(t) = \hat{W}(x^*(t),t)$, $u^*(t) = \hat{U}(x^*(t), w^*(t), t)$, $x^*(t+1) = f(x^*(t), u^*(t), w^*(t))$, and $x^*(0) = x_0$ is a feedback Stackelberg equilibrium pair.

The feedback Stackelberg policy of the second player $\hat{U}(x,w,t)$ is the optimal strategy in the game defined over a finite horizon with total of $T-1$ moves. As in MPC, we induce a receding horizon control policy based on the first move [25]

$$U_{\mathrm{GT}}(x,w) \in \hat{U}(x,w,0). \quad (8)$$

The numerical implementation of updates (3)–(7) is similar to the ones in DDP and SDP. It can be based on backward-in-stage updates of the "cost-to-go" function over the mesh of quantized values for x, u, and w or on linear programming techniques. As in MPC, the selection of T is a design choice. The updates (3)–(7) in the GT case are simpler than SDP updates since the value function does not depend on w and T need not be very long. The reader is referred to [25] for additional remarks on connections between feedback Stackelberg equilibria and other notions of equilibria in GT (such as Nash equilibrium).

In the case of HEV, the control policy (8) can be directly implemented online using the feedforward terms of the wheel speed and wheel torque as w and the feedback term of SoC as x. To the extent that (2) is drive-cycle independent, the control policy (8) is drive-cycle and time independent; it can be evaluated and applied to any drive-cycle.

In terms of numerical implementation, the GT approach is similar to DDP. Hence the curse of dimensionality limits the applicability of the GT to models with low state and control dimensions. In typical cases of powertrain applications, time scale decomposition of the dynamics is present, which permits replacement of fast states in the model with static maps and regressions. In addition, the optimization can be performed over a finite number of predefined control policies (called modes) instead of a gridded control vector. Finally, the use of vectorized updates can speed up the implementation of the iterations (3)–(7) in MATLAB [21]. These observations lead to practical strategies to deal with the curse of dimensionality [23], [24] that will also be exploited in this paper.

TABLE I
ENGINE STATE FOR CISG AND ERAD MODES

		ERAD		
		Regen	Inactive	Drive
CISG	Regen	—	ON	—
	Inactive	OFF	ON	OFF
	Drive	—	ON	ON

To accommodate change of mind operation, the engine may still be connected to the wheel during the initial part of regen at high speed. In this scenario, the CISG will provide the regenerative braking torque.

TABLE II
EURO 4 DIESEL CLASS 3 VEHICLE STANDARDS

NO_x	0.39 g/km
HC + NO_x	0.46 g/km
CO	0.74 g/km

IV. PARALLEL HEV PROTOTYPE AND CONVENTIONAL VEHICLE EMULATOR

The parallel HEV prototype (Figs. 1 and 9 and [11]) is based on a conventional vehicle with a 2.2-L diesel engine and an automatic transmission. The main change to the powertrain is the replacement of the automatic transmission by a prototype six-speed dual clutch transmission, in which a crankshaft integrated starter generator (CISG) is placed between the flywheel of the 2.2-L diesel engine and the clutches.

Another electric motor is integrated in the rear of the vehicle within the differential and is permanently geared with the rear axle. This motor is called the electric rear axle drive (ERAD).

Table I summarizes feasible hybrid powertrain operating modes that are considered in the control strategy development. These modes correspond to different combinations of CISG and ERAD operating states: 1) regen; 2) inactive; and 3) drive.

In addition to the modes considered above, the powertrain is capable of operating in several other modes. These modes include a series mode, in which the engine and CISG generate power and directly drive the ERAD and a parallel mode with engine and ERAD both delivering power to the wheels. These modes are not considered because of the concerns with the efficiency losses, drivability, and degraded noise vibration and harshness (NVH) that emerged after their preliminary study during the vehicle development.

The emission targets to be achieved with this vehicle over the NEDC are based on EURO 4 diesel class 3 vehicle standards (see Table II).

The gearbox used on the prototype vehicle (Table III) is different from the gearboxes used on conventional donor vehicles. The gear-shifting map in our vehicle is optimized to

TABLE III
PROTOTYPE HEV GEARBOX RATIO

Gear	1	2	3	4	5	6
Ratio	3.655	2.368	1.754	1.323	1.009	0.775

The front final drive ratio of the Freelander 2 HEV is 4.063.

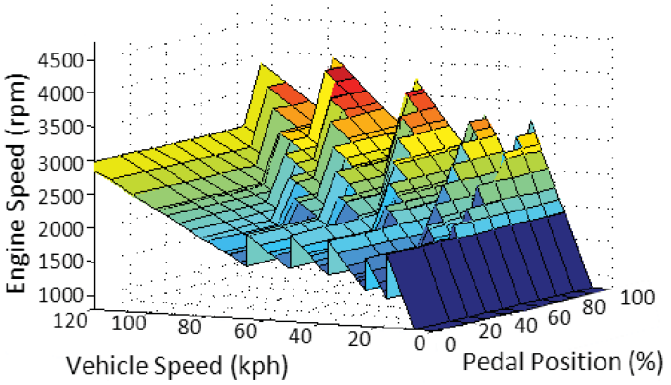

Fig. 2. Gear-shifting map chosen for prototype HEV.

shift in a range favorable to reduce NO_x and CO_2 emissions. Fig. 2 shows the upshift map chosen for the vehicle.

In this paper, we do not pursue simultaneous optimization of the gear shifts and battery power output. While there are benefits to including gear selection in the optimization, which can be demonstrated for idealized problem settings, in practice, there are multiple constraints, including drivability/drive feel, that significantly complicate numerical optimization-based approaches to shift optimization, even for conventional vehicles. Thus, we leave the GT-based approach to simultaneous optimization of the battery power output and gear shifts as a topic for future work.

Compared with the conventional vehicle, the prototype HEV has a new engine, a prototype gearbox, and in our experimental setup, it is connected to instrumentation and rapid prototyping equipment for the controller. These are run off the low-voltage system to allow on-road tests.

The baseline (conventional) vehicle for the subsequent comparison of fuel economy and emissions is emulated by the same prototype HEV while running in an engine-only mode with a feedback loop on the CISG torque acting as an alternator to sustain the energy drained by the 12 V system over the cycle. In addition, a lighter road load is applied to replicate the mass and loads of the conventional diesel vehicle. Because of these differences between vehicle prototype and production variants (as well as proprietary concerns), here and later, in this paper, we report incremental changes in fuel consumption, emissions, and battery charge between different options rather than absolute numbers. This emulation of the conventional vehicle is implemented both in the experimental setup and in the model simulations.

Using this gear-shifting map, the trajectories of wheel speed, wheel torque, and gear over NEDC are determined (see Fig. 3). These trajectories are used in computing DDP solutions and in tuning parameters of the cost function of the GT controller.

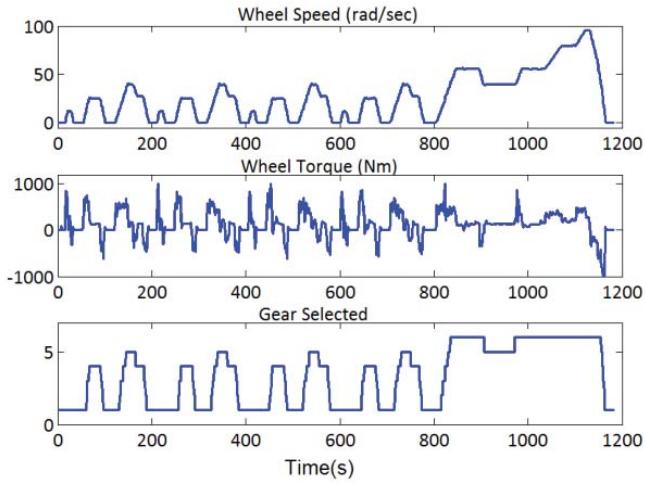

Fig. 3. Time histories of wheel speed (rad/s), wheel torque (Nm), and gear selected over NEDC.

V. PREVIOUS FUEL ECONOMY OPTIMIZATION RESULTS

In [11], we consider a dynamic optimization problem of minimizing fuel consumption subjected to charge sustainability constraints. Five approaches (two conventional and three based on dynamic optimization) are compared using a detailed HEV simulation model. The two conventional approaches are based on the BOPOM and on a RB control. The three advanced controllers are based on the DDP, GT, and SDP. For the three advanced controllers, the control policies prescribe the powertrain operating mode (out of six possible modes that include EV mode, engine only mode, two charging modes, and two boosting modes) while the incremental cost is based on a weighted sum of fuel consumption and a penalty on the SoC deviation from the set-point. An additional penalty term for the deviation of wheel speed and wheel torque is added in [11] to the incremental cost function in GT controller. The control policies are computed offline using MATLAB running on Intel Pentium M 2-GHz PC with 1 GB of RAM. It took $\sim$190 times longer to compute the SDP policy than the GT policy, and it took six times longer to compute the GT policy than the DDP policy.

Table IV summarizes the fuel consumption results we obtained in simulations with different controllers over NEDC, where the columns are arranged in the order of increasing benefit. Based on the results of this evaluation, the BOPOM controller, calibrated to approximately replicate the DDP trajectories over NEDC, is retained as the baseline strategy, and the GT controller is retained for further development and experimental implementation in the vehicle. Compared with [11], in this paper (and partly in [12]), the GT controller is expanded with additional modes; the NO_x emissions are included in the optimization, and experimental assessment and validation in vehicle prototype are completed.

VI. DESKTOP OPTIMIZATION SETUP

For the development of DDP trajectories and the GT controller, a control-oriented model of the prototype HEV is implemented. This model has the following components:

TABLE IV
FUEL CONSUMPTION SUMMARY

	RB	BOPOM	SDP	GT	DDP
Fuel consumption (L/100 km)	5.93	5.92	5.7	5.46	5.35
Fuel saving compared with conventional vehicle (%)	20.9	21.1	24	27.2	28.7

Comparison of fuel consumption improvement opportunities versus the conventional vehicle over NEDC for five energy management approaches [11]: RB, BOPOM, SDP, GT, and DDP.

1) steady-state engine outputs: NO_x and brake-specific fuel consumption;
2) CISG motor/generator and inverter efficiency;
3) ERAD motor/generator and inverter efficiency;
4) gearbox efficiency;
5) battery efficiency;
6) battery SoC as a dynamic state.

A discrete set of modes is then defined based on feasible powertrain operating modes.

1) EV mode, where only ERAD is used to satisfy the driver torque demand at the wheel.
2) Engine-only mode, where the torque demand from the electric machines is set to 0 Nm.
3) EV to parallel mode, which is introduced to reflect the penalty in terms of fuel consumption and emissions of starting the engine.
4) A set of four parallel charging modes, where CISG torque is set to a negative torque (between -80 and -20 Nm with a step of 20 Nm), while the engine provides the driver-demanded torque plus the CISG torque.
5) A set of four boosting modes, where the CISG torque is set to a defined positive torque (between 20 and 80 Nm with a step of 20 Nm), and the engine fills in for the rest of the driver demanded torque.

In addition, in the case of negative wheel torque request, the system can switch to a regenerative braking mode, where the ERAD recharges the battery within system limits.

VII. CALIBRATING BOPOM STRATEGY USING DYNAMIC PROGRAMING AND TESTS ON CHASSIS DYNAMOMETER

A. Baseline BOPOM Controller

The BOPOM controller is a baseline strategy used in our prototype HEV. The BOPOM controller uses a map of battery power, either requested from the battery (if with positive sign) or provided to the battery (if with negative sign), given wheel speed and battery SoC. See Fig. 4 for an example of this map. If the power specified by this map is positive, the battery delivers the requested power to ERAD in the EV mode or to CISG in a parallel mode. In a parallel mode, the engine complements battery power as needed to meet the wheel torque request. If BOPOM prescribes negative battery power, the battery is to be charged. The engine and CISG are operated so that the excess power is provided to recharge the battery

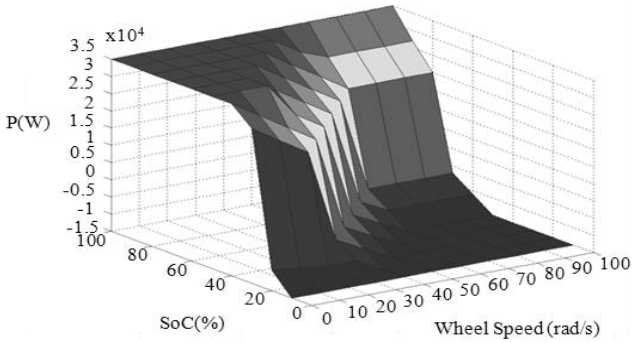

Fig. 4. Battery power output (W) map as a function of battery SoC (0%–100%) and wheel speed (0–100 rad/s).

(if possible) and the driver requested torque is delivered at the wheels.

Additional logic is implemented in the controller to ensure that the value of the battery output power map will be limited not to exceed the driver demand.

In the case of negative wheel torque requests, this map is not used and the system switches to regenerative braking mode, where the ERAD recharges the battery within system limits.

The BOPOM strategy is tuned using optimal DDP trajectories for NEDC. These trajectories are generated offline using a simulation model. Then the resulting BOPOM controller is evaluated in vehicle experiments and ultimately compared with GT controller.

B. Offline DDP Solution

The dynamic programing uses the incremental cost function of the form

$$L(x,u,w) = \alpha \cdot \text{Fuel} + \beta \cdot \text{NO}_x + \mu \cdot [\text{SoC}_{\text{SetPoint}} - \text{SoC}]^2 \quad (9)$$

where $u \in U$ is the control (powertrain operating mode in our case), $x \in X$ is the state (high voltage battery SoC in our case) and $w \in W$ is the vector of operating variables, which we refer to as the "operating point" (wheel speed, wheel torque and gear selected in our case). In (9), $\text{Fuel} = \text{Fuel}(x,u,w)$ denotes engine fuel consumption (in g/s), $\text{NO}_x = \text{NO}_x(x,u,w)$ denotes engine NOx emissions mass flow rate (in g/s), $\text{SoC}_{\text{SetPoint}}$ denotes the desired SoC set-point (in %), which is determined by a higher level controller, and $\text{SoC} = \text{SoC}(x,u,w)$ denotes the SoC (in %).

To maintain SoC near the requested set-point, the cost function includes a quadratic term on SoC deviation. This limits the charge and discharge cycle of the high-voltage battery, thereby improving battery durability and battery life. Battery durability and battery life extension are critical requirements in our vehicle development.

Cost function (9) can also include a penalty for HC and a penalty for CO emissions; this approach is not pursued as emissions of HC and CO are meeting the requirements for our powertrain.

The numerical solution of DDP uses 1% SoC mesh and exact values of wheel speed and wheel torque versus time. The weights α, β, μ are adjusted using several optimizations

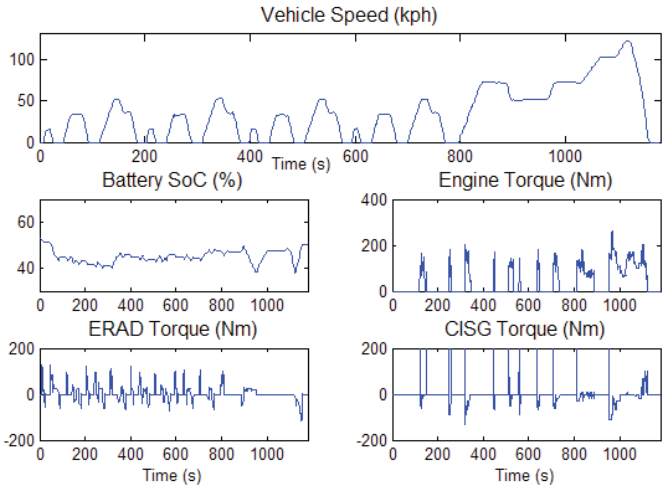

Fig. 5. Simulation results of DDP solution for the prototype HEV over NEDC.

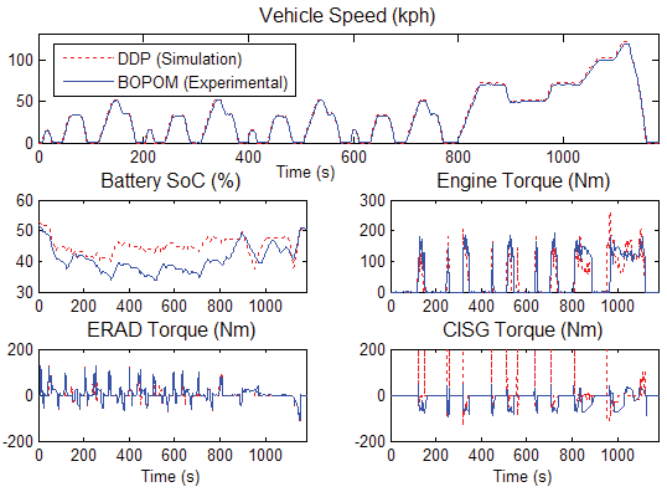

Fig. 6. Experimental behavior of prototype vehicle on the chassis dynamometer over NEDC (solid line) with BOPOM versus (dashed line) DDP simulation results.

and simulations to ensure an emission compliant and charge balancing solution with best fuel economy. The optimal trajectories generated by the DDP algorithm and simulated using the prototype HEV model are shown in Fig. 5.

A simulated NO_x EURO4 compliant solution gives 25% CO_2/fuel consumption savings as compared with the emulated conventional vehicle. This 25% EURO4 improvement is obtained with a strategy calibrated to reduce mode chattering between EV mode and parallel mode (see [12] for further details) and hence with similar level of drivability to that of the conventional vehicle.

C. BOPOM Calibration and Test on Prototype Vehicle

The BOPOM controller is initially calibrated to provide the vehicle with the behavior that replicated the DDP solution over NEDC, including start/stop and battery charge/discharge by the engine. Further calibration adjustments are made to reduce transient emissions not accounted for to a sufficient extent in the DDP optimization that used steady-state emissions maps.

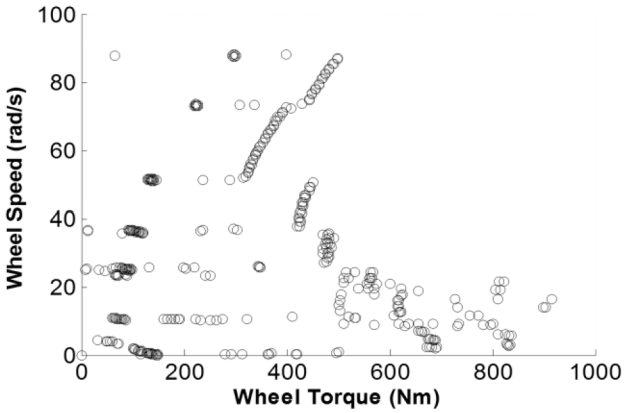

Fig. 7. HEV prototype operating points over NEDC.

Fig. 6 shows the time histories of vehicle variables over NEDC and compares experimental results obtained with the BOPOM controller to DDP simulation results. Unlike simulated DDP trajectories, the BOPOM controller in the vehicle uses CISG less aggressively and balances the SoC on the extra urban part of the cycle with the increased charging demand. The differences are also partly attributed to the battery model used for optimization, which is not a perfect match to the battery installed in the prototype. The battery dynamics are essentially that of an integrator and hence can drift.

The BOPOM controller demonstrated a 21.5% CO_2 saving over NEDC compared with the emulated conventional vehicle, is EURO4 compliant, and the SoC is balanced over the cycle.

VIII. GT Controller Implementation and Testing on Chassis Dynamometer

The GT controller used the following incremental cost function:

$$L(x,u,w) = \alpha \cdot \text{Fuel} + \beta \cdot \text{NO}_x + \mu \cdot [\text{SoC}_{\text{SetPoint}} - \text{SoC}]^2 + \gamma \cdot G(w) \quad (10)$$

where $\text{Fuel} = \text{Fuel}(u,w)$, $\text{NO}_x = \text{NO}_x(u,w)$, $u \in U$, $x \in X$ and $w \in W$ have the same meaning as in the previous section The dynamics of SoC are the battery dynamics given by (1). The last term in (10), $\gamma \cdot G(w)$, is a penalty on the deviations of the vehicle operating variables from conditions expected over typical drives. In generating the GT controller, we choose G as a positive bell-shaped function. The introduction of G focuses the optimization on the region where typical operating conditions are expected to occur rather than on the worst-case operating conditions. See Fig. 7, which delineates the prototype HEV operating points over NEDC, and Fig. 8, which illustrates the selected $G(w)$. Note that $G(w)$ takes large values near locations where we expect the vehicle to operate over typical driving cycles.

The GT controller is based on feedback Stackelberg equilibrium of the game constructed offline, where after experimenting with several choices in simulation, the horizon of the game (Section III) is chosen so that $T = 4$. This choice of the horizon provided the best tradeoff between performance

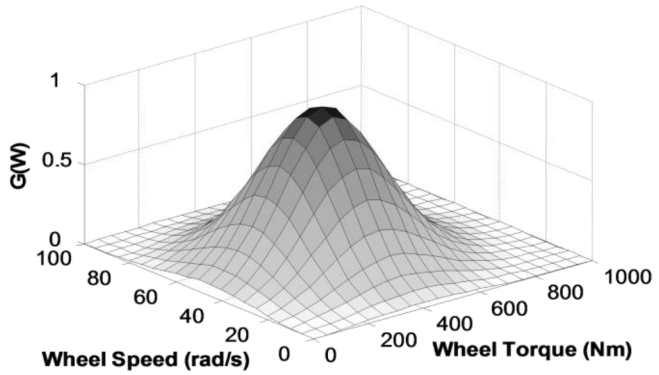

Fig. 8. Bell-shaped function $G(w)$ in the cost (10).

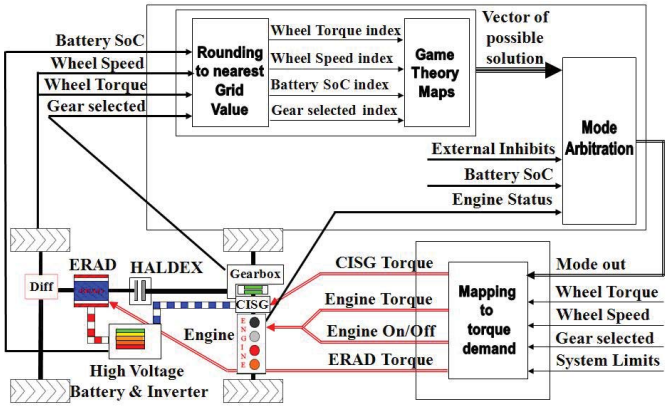

Fig. 9. HEV energy management controller based on GT.

on NEDC and robustness off NEDC. It also has an added advantage of requiring shorter (offline) computing time than the solutions with longer horizons.

The GT controller $U_{\mathrm{GT}}(x, w)$ is implemented as a set of offline computed maps based on grids for state, control, and operating point values. It uses online interpolation and generates the control action that defines the powertrain operating mode. A more detailed description of the implementation of this controller in the prototype HEV is given in the following section.

A. Vehicle Hybrid Supervisory Controller Based on GT

The overall structure of the hybrid supervisory controller that uses GT maps for energy management is based around three main modules as follows:

1) GT maps module;
2) mode arbitration module;
3) mapping to torque demand module.

These modules rely on the offline calibration of the GT maps and an appropriate set of inputs from the vehicle to determine which mode, within given drivability constraints, is to be used at any time instant of the drive. Fig. 9 shows the inputs and outputs of each of the controller modules/blocks. Further description of these modules is given as follows.

1) GT Maps: Rounding to nearest grid value block in Fig. 9 is responsible for discretizing the input of the controller, specifically wheel torque and speed, gear selected, and battery SoC. This block outputs indexes that identify relevant operating point and states of the system in the offline calibrated GT maps.

The output of GT maps module consists of two modes from which one mode is chosen during mode arbitration based on additional logic conditions.

2) Mode Arbitrator: The mode arbitrator module selects one mode from the two mode outputs of GT maps module or, under certain conditions, overrides mode outputs entirely. Normally, the first mode output of GT maps is used but if, for instance, the engine has just started, the mode arbitrator will not activate EV mode even if it is identified as optimal by GT maps module; instead the second mode output from the GT maps module (a parallel mode in this case) will be used.

In addition, the mode arbitrator module deals with drivability issues, such as suppressing the chattering behavior between EV mode and parallel modes.

In more detail, if the engine is just turned on, a timer may keep the engine on for a defined period, unless the driver releases the pedal for a speed dependent period or presses on the brake pedal, in which condition the controller allows transitioning back into EV mode before expiry of the engine-on timer. The same principle applies when transitioning out of the EV mode, an engine start is delayed by a certain amount of time unless the driver request starts exceeding the capability of the electric machine.

The mode arbitrator also allows to deal with specific conditions such as low-battery SoC and driver behavior detection and accommodation. Specifically:

a) in the case of an aggressive driver, the controller detects the driver behavior and requests aggressive SoC charging to avoid performance fading;
b) in the case of a low battery SoC, a moving SoC charging latch is used to accommodate traffic condition and reduce fast switching between engine on/off states that can degrade vehicle drivability.

Mode arbitrator also handles other specific modes required for our vehicle, such as exhaust after treatment warm-up mode and engine NVH modes, where high charge demand is inhibited in defined conditions.

3) Mapping to Torque Demand: The mapping to torque demand module is responsible for splitting the torque between the engine and the electrical machine(s), as requested by the output of the mode arbitrator module. By accounting for the component dynamics, this module avoids sudden driveline jerk and wheel torque disturbances/fluctuations.

The mapping to torque demand module also deals with the transient events to provide torque filling, if desired, in specific conditions such as the diesel engine experiencing turbo lag because of smoke limiting.

Finally, this module also provides smooth transition between parallel and EV modes, along with dealing with system limits.

TABLE V
HEV PROTOTYPE GEARBOX INPUT TORQUE FOR GT OPTIMIZATION

Gear selected	1	2	3	4	5	6
Gearbox input Torque	0–67	0–104	0–140	0–186	0–244	0–318 Nm

Range of gearbox input torque is given as a function of the gear selected.

B. Generation of GT Maps and Complexity Reduction

To address the memory constraints of the electronic control unit (ECU), a parametric study is conducted to select the adequate resolution grid of each input and output. The selection is based on the performance-complexity tradeoff and requirements to cover driving conditions over which the HEV prototype is tested (which covers most of real-world driving conditions). The resulting grids are as follows.

1) *Wheel Torque:* The range of the wheel torque for which the optimization is performed is 0–1000 Nm and the mesh uses a 50-Nm step. This covers the range of the gearbox input torque described in Table V.
2) *Wheel Speed:* The range of the wheel speed on which the optimization is performed is 0–100 rad/s and the mesh uses a 5 rad/s step. This covers the range of the gearbox input speed between 0 and 4000 rpm, from gear 1–5 to 0–3000 rpm for gear 6.
3) *Battery SoC:* The range of SoC exploited in the vehicle is between 40% and 70%, while the mesh is selected with the step of 5%. This discretization of the SoC is coarser than in DDP to reduce online memory requirements. Hysteresis is implemented on SoC signal to ensure that fast mode switches and rapid cycling of the battery between charging and discharging are avoided during cruise conditions.
4) *Gear Selected:* This is already a discrete variable that can take one of six values corresponding to each of the forward gears available.

The selected ranges of wheel torque and wheel speed ensured that in most of the cases, when in parallel mode, the engine load can be shifted from an inefficient or nonemission compliant operating region to a region where an adequate tradeoff between brake specific fuel consumption and emission is achieved.

The memory requirements of the controller are dictated by the size of GT maps that use the following:

1) twenty-one discrete wheel torque values;
2) twenty-one discrete wheel speed values;
3) seven discrete SoC values;
4) six discrete gears;
5) two outputs.

Based on 11 modes available for each combination of input, the implementation of the maps within the prototype ECU requires 37 kB. Based on the use of a combinatorial compression technique, the size of the GT maps is further reduced to 18.61 kB without impacting the ECU chronometric loading.

TABLE VI
BOPOM VERSUS GT OVER NEDC

NEDC results improvement over baseline conventional vehicle	BOPOM (%)	GT (%)
CO_2	21.5	22.5
NO_x	0	11.1
Cycle ΔSoC	−1	−2

Results are compared with the baseline vehicle for CO_2 and NO_x. The BOPOM controller is calibrated to replicate operation of the offline optimal DDP solution over NEDC and is not calibrated for real-world drivability, while the GT controller uses offline calibrated maps and the controller is calibrated to enhance real-world drivability; the conventional vehicle is the prototype running with a lighter road load and using the CISG to sustain the 12-V loads.

C. Controller Calibration Process on the Prototype Vehicle

The calibration of the controller is performed in two stages.

1) The calibration of the drivability part of the controller (mode arbitrator, mapping to torque demand, and so on) on the track.
2) The offline calibration of the GT maps by adjusting weights for the cost function to reduce fuel consumption and satisfy emissions constraints as well as charge sustainability requirements over NEDC.

A few iterations of this calibration process are normally needed to address any discrepancy observed between the vehicle on the chassis dynamometer and the simulation model. Three or four iterations are usually sufficient to obtain a robust and efficient calibration of the GT maps such that drivability requirements are satisfied. This iterative process, which involves model-based development, reduces the number of experimental tests on the chassis dynamometer and is proven to be an efficient way to reduce calibration costs.

The GT controller tuned using this calibration process delivered 22.5% reduction in CO_2 over NEDC compared with the baseline vehicle while achieving a high level of drivability refinement adequate for real-world driving conditions.

D. Performance of GT Controller Versus BOPOM Controller Over NEDC

Table VI compares CO_2 emissions (equivalent to fuel consumption), NO_x emissions, and charge sustainability of DDP-calibrated BOPOM and GT controller. The GT controller demonstrates better fuel economy and substantially better NO_x emissions as compared with the BOPOM controller calibrated from DDP results.

Fig. 10 shows that the GT-based controller delivers a tighter control of the SoC over NEDC than the BOPOM controller but allows for more torque assist from the electric machine at high torque demand values; this resulted in a 1% SoC deficit of the GT controller against the BOPOM controller at the end of the cycle. This tighter control of SoC is possible because of the GT decision being torque and speed based, allowing for a more accurate tracking of the nonlinearity of the engine emissions than was possible with the power-based BOPOM strategy.

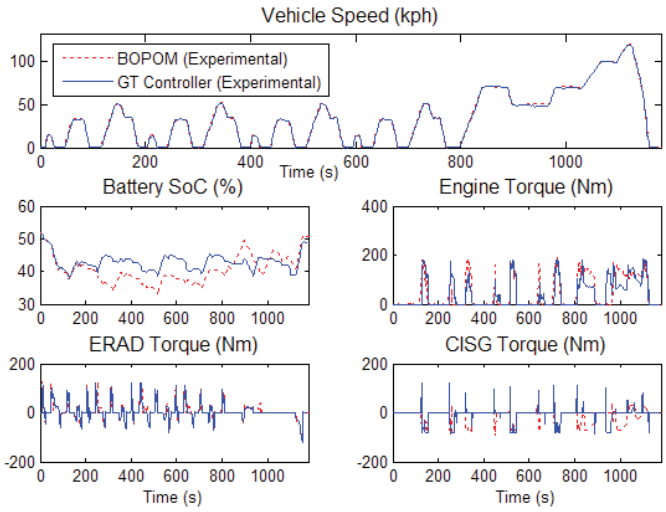

Fig. 10. Time histories of prototype HEV variables on chassis dynamometerover NEDC: with GT-based controller (solid line) and with BOPOM controller calibrated from dynamic programing results (dashed line).

TABLE VII
BOPOM VERSUS GT OVER NEDC, FTP75, AND HYZEM PHASE 2

Drive Cycle	Output	GT Performances Versus BOPOM (%)
NEDC	CO_2	−4.5
	NO_x	−11.1
	Cycle ΔSoC	−1.0
FTP75	CO_2	−0.2
	NO_x	−7.3
	Cycle ΔSoC	+0.2
HYZEM Phase 2	CO_2	−4.5
	NO_x	−4.0
	Cycle ΔSoC	+1.1

Performance of GT controller versus BOPOM controller. The BOPOM controller is calibrated to replicate operation of the offline optimal DDP solution over NEDC and is not calibrated for real-world drivability, while the GT controller uses offline calibrated maps and the controller is calibrated to enhance real-world drivability with NEDC SoC balance focus.

E. Assessment of BOPOM and GT Controller Robustness on Chassis Dynamometer Over Different Drive-Cycles

The GT controller is drive-cycle independent as it does not assume known vehicle speed/road trajectory (as in DDP or MPC with a preview) or their statistics (as in SMPC or SDP approaches of [30] and [34]) over the effective prediction horizon.

Hence, we expect that the GT controller can perform well over drive-cycles other than NEDC and perform better than BOPOM controller calibrated using dynamic programing optimization on the NEDC.

The two controllers are benchmarked against each other over NEDC, the hybrid technology approaching efficient zero emission mobility (HYZEM) cycle phase 2 (urban phase) [29] and the federal test procedure drive-cycles (FTP75), developed by the U.S. Environmental Protection Agency for certification of passenger vehicles. The results are summarized in Table VII. It can be observed that over three different drive-cycles, the GT controller, that is calibrated to balance charge over NEDC, with very limited calibration effort, provides better fuel economy, NO_x emissions, and SoC control than the baseline BOPOM controller calibrated for a specific drive-cycle using trajectories obtained with the help of optimal control theory. The capability of the GT controller to reduce NO_x emissions while simultaneously improving fuel economy is of significant interest for our vehicle configuration that does not have NO_x after treatment.

F. Drivability

The fuel economy and NO_x emission results reported in Table VI are for the calibration of GT controller that is refined on the test track to provide acceptable real-world drivability on public road. Specifically, the calibration of mode arbitrator and mapping to torque demand functionality is improved to avoid issues such as frequent or unexpected switching between engine on and off states. The BOPOM controller provides acceptable drivability on NEDC; however, its drivability on public road off NEDC is not refined nor even acceptable. It is subjectively characterized as occasionally odd and unpleasant. Generally, imposing real-world drivability constraints degrades fuel economy and emission benefits. Therefore, our approach to assessing the incremental fuel economy and emission benefits of the GT controller may be viewed as conservative, thus avoiding overly optimistic projections. Our previous simulation results (reported in [11] and reviewed in Section V) are for the GT controller that did not reflect the drivability refinements and did not include NO_x penalty in the cost; this and the inherent model to test variability account for the observed differences between simulated and experimental fuel economy and emission results.

IX. CONCLUSION

This paper described the development of an HEV energy management controller based on the application of the GT. In this approach, vehicle operation was viewed as a noncooperative game between the driver and the powertrain. As compared with DDP, the direct application of which provided optimal (with respect to a chosen cost functional) trajectories that explicitly depend on time and the specific drive-cycle, the GT approach generated control policies that were time independent, cycle independent, and thus implementable. As compared with SDP, the offline computations were simpler in the GT case as the value function depended on fewer variables (specifically, it does not depend on operating variables).

This paper presented the results of the experimental evaluation of the GT controller. This controller was calibrated to provide high level of refinement with respect to real-world drivability and to be SoC neutral (within acceptable tolerance) over NEDC.

The GT controller in-vehicle performance, in terms of fuel consumption, NO_x emissions, and drivability, was compared with the BOPOM controller calibrated from the optimal control trajectories over NEDC without focusing on real-world drivability. The GT controller provided better fuel economy

along with improved emissions and drivability over several driving cycles. The vehicle drivability with the GT controller was also adequate on public road. These results highlighted the robustness of the controller.

Our approach to designing a GT controller was based on the feedback Stackelberg equilibrium framework, a specific selection of a cost function to penalize fuel consumption, NO_x emissions, SoC deviations and deviations of the operating conditions, and appropriate tuning of the weights in this cost. This approach was demonstrated to lead to a successful solution to HEV energy management problem that was confirmed with extensive vehicle validation results. The calibration process, while it involved some iterations between offline and in-vehicle tuning steps, was relatively straightforward. Ancillary parts of the controller, augmented to handle real-world drivability requirements, were discussed. Based on these results, the GT controller was adopted as an integral part of the future Jaguar Land Rover hybrid vehicle line.

Many strategies were proposed for control and energy management of HEVs. Although our comparison was with a specific baseline controller, that represented an agreed benchmark for our vehicle, the development, implementation, and comparison with other strategies, including those proposed in the last five years (e.g., [5], [8], [18], [20], [22], [30], [31], [34], [35], and references therein) represents a topic of continuing research.

REFERENCES

[1] J. E. Auiler, J. D. Zbrozek, and P. N. Blumberg, "Optimization of automotive engine calibration for better fuel economy: Methods and applications," in *Proc. Soc. Auto. Eng. World Congr.*, Detroit, MI, USA, Feb. 1977, no. 770076, pp. 1–17.

[2] T. Basar and G. J. Olsder, *Dynamic Noncooperative Game Theory*. Philadelphia, PA, USA: SIAM, 1982.

[3] D. P. Bertsekas, *Dynamic Programming: Deterministic and Stochastic Models*. Englewood Cliffs, NJ, USA: Prentice-Hall, 1987.

[4] D. P. Bertsekas and J. N. Tsitsiklis, *Neuro-Dynamic Programming*. Belmont, MA, USA: Athena Scientific, 1996.

[5] A. Brahma, Y. Guezennec, and G. Rizzoni, "Optimal energy management in series hybrid electric vehicle," in *Proc. Amer. Control Conf.*, Chicago, IL, USA, Sep. 2000, pp. 60–64.

[6] S. Di Cairano, W. Liang, I. V. Kolmanovsky, M. L. Kuang, and A. M. Phillips, "Power smoothing energy management and its application to a series hybrid powertrain," *IEEE Trans. Control Syst. Technol.*, to be published.

[7] C. C. Chan, "The state of the art of electric, hybrid, and fuel cell vehicles," *Proc. IEEE*, vol. 95, no. 4, pp. 704–718, Apr. 2007.

[8] A. Chasse and A. Sciarretta, "Supervisory control of hybrid powertrains: An experimental benchmark of offine optimization and online energy management," *Control Eng. Pract.*, vol. 19, no. 11, pp. 1253–1265, 2011.

[9] A. Cohen, K. Randall, C. Tether, K. Van Voorhies, and J. Tennant, "Optimal control of cold automobile engines," in *Proc. Soc. Autom. Eng. World Congr.*, Detroit, MI, USA, 1984, no. 840544, pp. 1–11.

[10] C. Dextreit, F. Assadian, I. V. Kolmanovsky, J. Mahtani, and K. Burnham, "Approaches to optimisation of energy management in a hybrid electric vehicle," in *Proc. 16th Int. Conf. Syst. Sci.*, vol. 3. Sep. 2007, pp. 67–78.

[11] C. Dextreit, F. Assadian, I. V. Kolmanovsky, J. Mahtani, and K. Burnham, "Hybrid electric vehicle energy management using game theory," in *Proc. Soc. Autom. Eng. World Congr.*, Detroit, MI, USA, Apr. 2008, no. 2008-01-1317, pp. 1–12.

[12] C. Dextreit and I. V. Kolmanovsky, "Approaches to energy management of hybrid electric vehicles: Experimental comparison," in *Proc. UKACC Int. Conf. Control*, Sep. 2010, pp. 4710–4715.

[13] Y. Ehsani, Y. Gao, and J. M. Miller, "Hybrid electric vehicles: Architecture and motor drives," *Proc. IEEE*, vol. 95, no. 4, pp. 719–728, Apr. 2007.

[14] O. Grondin, L. Thibault, P. Moulin, A. Chasse, and A. Sciarretta, "Energy management strategy for diesel hybrid electric vehicle," in *Proc. IEEE Vehicle Power Propuls. Conf.*, Chicago, IL, USA, Sep. 2011, pp. 1–8.

[15] L. Guzzella and A. Sciarretta, "Control of hybrid electric vehicles: Optimal energy management strategies," *IEEE Control Syst. Mag.*, vol. 27, no. 2, pp. 60–70, Feb. 2007.

[16] B. Jacobson and M. Spickenreuther, "Gearshift sequence optimization for vehicles with automated non-powershifting transmissions," *Int. J. Vehicle Design*, vol. 32, nos. 3–4, pp. 187–207, 2003.

[17] L. Johannesson, M. Asbogard, and B. Egardt, "Assessing the potential of predictive control for hybrid vehicle powertrains using stochastic dynamic programming," *IEEE Trans. Intell. Trans. Syst.*, vol. 8, no. 1, pp. 71–83, Mar. 2007.

[18] L. Johannesson, S. Pettersson, and B. Egardt, "Predictive energy management of a 4QT series-parallel hybric electric bus," *Control Eng. Pract.*, vol. 17, no. 12, pp. 1440–1453, Dec. 2009.

[19] V. Johnson, K. Wipke, and D. Rausen, "HEV control strategy for real-time optimisation of fuel economy and emissions," in *Proc. SAE World Congr.*, Detroit, MI, USA, Apr. 2000, no. 2000-01-1543, pp. 1–15.

[20] R. Johri and Z. Filipi, "Self-learning neural controller for hybrid power management using neuro-dynamic programming," in *Proc. SAE World Congr.*, Detroit, MI, USA, Sep. 2011, no. 2011-24-0081, pp. 1–16.

[21] J.-M. Kang, I. Kolmanovsky, and J. Grizzle, "Approximate dynamic programming solutions for lean burn engine after treatment," in *Proc. 38th IEEE Conf. Decision Control*, vol. 2. Phoenix, AZ, USA, Jan. 1999, pp. 1703–1708.

[22] S. Kermani, S. Delprat, T. M. Guerra, R. Trigui, and B. Jeanneret, "Predictive energy management for hybrid vehicle," *Control Eng. Pract.*, vol. 20, no. 4, pp. 408–420, Apr. 2012.

[23] I. Kolmanovsky, M. Van Nieuwstadt, and J. Sun, "Optimization of complex powertrain systems for fuel economy and emissions," *Nonlinear Anal., RWA*, vol. 1, pp. 205–221, Jun. 2000.

[24] I. Kolmanovsky, S. Sivashankar, and J. Sun, "An integrated software environment for powertrain feasibility assessment using optimization and optimal control," *Asian J. Control*, vol. 8, no. 3, pp. 199–209, Mar. 2006.

[25] I. Kolmanovsky and I. Sivergina, "Feasibility assessment and operating policy optimization of automotive powertrains with uncertainties using game theory," in *Proc. ASME Int. Mech. Eng. Congr. Exposit.*, New York, NY, USA, Nov. 2001, pp. 1–8.

[26] I. Kolmanovsky, I. Sivergina, and B. Lygoe, "Optimization of powertrain operating policies for feasibility assessment and calibration: Stochastic dynamic programming approach," in *Proc. Amer. Control Conf.*, Anchorage, AK, USA, May 2002, pp. 1425–1430.

[27] N. N. Krasovskii and A. I. Subbotin, *Game Theoretical Control Problems*. New York, NY, USA: Springer-Verlag, 1988.

[28] C. Lin, H. Peng, and J. Grizzle, "A stochastic control strategy for hybrid electric vehicles," in *Proc. Amer. Control Conf.*, vol. 5. Boston, MA, USA, Jul. 2004, pp. 4710–4715.

[29] A. Michel, *European Development Of Hybrid Technology Approaching Efficient Zero Emission Mobility (Hyzem): Driving Patterns Analysis And Driving Cycles*. Beranger, Paris, France, 1997.

[30] D. Opila, X. Wang, R. McGee, R. B. Gillespie, J. Cook, and J. W. Grizzle, "An energy management controller to optimally trade off fuel economy and drivability for hybrid vehicles," *IEEE Trans. Control Syst. Technol.*, vol. 20, no. 6, pp. 1490–1505, Nov. 2012.

[31] A. Phillips, R. McGee, J. Lockwood, R. Spiteri, J. Che, J. Blankenship, and M. Kuang, "Control system development for the dual drive hybrid system," in *Proc. SAE World Congr.*, Detroit, MI, USA, 2009, no. 2009-01-0231, pp. 1–9.

[32] D. Prokhorov, "Approximating optimal controls with recurrent neural networks for automotive systems," in *Proc. IEEE Conf. Control Appl.*, Jul. 2007, pp. 669–680.

[33] D. Prokhorov, "Training recurrent neuron-controllers for real-time applications," *IEEE Trans. Neural Netw.*, vol. 18, no. 4, pp. 1003–1015, Jul. 2007.

[34] G. Ripaccioli, D. Bernardini, S. Di Cairano, A. Bemporad, and I. V. Kolmanovsky, "Stochastic model predictive control approach for a series hybrid electric vehicle power management," in *Proc. Amer. Control Conf.*, Baltimore, MD, USA, Jul. 2010, pp. 5844–5849.

[35] M. Sorrentino, G. Rizzo, and I. Arsie, "Analysis of a rule-based control strategy for on-board energy management of series hybrid vehicles," *Control Eng. Pract.*, vol. 19, no. 12, pp. 1433–1441, Dec. 2011.

[36] E. Tate, J. W. Grizzle, and H. Peng, "Shortest path stochastic control for hybrid electric vehicles," *Int. J. Robust Nonlinear Control*, vol. 18, no. 14, pp. 1409–1429, 2008.

[37] H. Von Stackelberg, *The Theory of the Market Economy*. London, U.K.: Oxford Univ. Press, 1952.
[38] N. N. Vorob'ev, *Game Theory: Lectures for Economists and Systems Scientists*. New York, NY, USA: Springer-Verlag, 1977.

Clément Dextreit received the French engineering Master degree from the ENSITM (now ENSISA), in 2004, and the M.Sc. degree in automotive engineering from the University of Coventry, Coventry, U.K., in 2005.

He is currently a Subject Matter Expert in energy management for hybrid vehicles at Jaguar Land Rover. In the past seven years, he has led the development of the hybrid supervisory controller energy management that has been used in a wide range of demonstrator vehicles from mild hybrid to plug-in hybrid electric vehicles (Range-e, XJ-e) and which is the core of the first commercial Land Rover hybrid vehicle. His current research interests include optimal and predictive control for advanced automotive systems.

Ilya V. Kolmanovsky (F'08) received the M.S. and Ph.D. degrees in aerospace engineering, and the M.A. degree in mathematics from the University of Michigan, Ann Arbor, MI, USA, in 1993, 1995, and 1995, respectively.

He is currently a Professor in the Department of Aerospace Engineering, University of Michigan. His research interests include control theory for systems with state and control constraints, control of automotive and aerospace propulsion systems, and spacecraft control applications. Prior to joining the University of Michigan, he was with Ford Research and Advanced Engineering, Dearborn, MI, USA, for almost 15 years.

Dr. Kolmanovsky was a recipient of the Donald P. Eckman Award of American Automatic Control Council, the IEEE TRANSACTIONS ON CONTROL SYSTEMS TECHNOLOGY Outstanding Paper Award, and several Ford Research and Advanced Engineering Technical Achievement, Innovation, and Publication Awards.